Asian Journal of Chemistry; Vol. 25, No. 3 (2013), 1307-1310

ASIAN JOURNAL OF CHEMISTRY

http://dx.doi.org/10.14233/ajchem.2013.12956

# Role of *n-n* Anatase-Rutile Heterojunction in the Photocatalysis of Mixed-Phase Titania

SONG LIU*, YANHONG YAN, WEIWEI GUAN, MINGZE LI and RONGYING JIANG

Department of Applied Chemistry, South China University of Technology, Guangzhou 510640, P.R. China

*Corresponding author: Fax: +86 20 87112906; Tel: +86 20 87114875; E-mail: chsliu@scut.edu.cn

(*Received*: 29 October 2011; *Accepted*: 8 September 2012) AJC-12103

The electric field distribution in the transition region of the *n-n* anatase-rutile heterojunction in mixed-phase titania is provided by solving the Poisson equation. The electrons flow from anatase to rutile when rutile contacts closely with anatase, creating an accumulation of negative charges in the rutile region and a positive section in the anatase region in the vicinity of the junction. This sets up an internal electrostatic field directed from the anatase region to the rutile region, creating an energy barrier for the electron transfer from anatase to rutile. Strong electric field exists in the transition region and can exert a very efficient force for photogenerated electron hole pair separation, resulting in greater photocatalytic activity. Once a stable *n-n* heterojunction has formed between rutile and anatase, under illumination, the photogenerated electrons will migrate from rutile to anatase while the photogenerated holes will migrate from anatase to rutile.

**Key Words: Inorganic materials, Oxide materials, Heterojunctions, Catalysis, $TiO_2$, Mixed-phase.**

## INTRODUCTION

Heterogeneous photocatalysis using $TiO_2$ has been considered as an effective technology for removing toxic and nonbiodegradable organic compounds in water and in air. Recently, it is has been found that a mixture of anatase and rutile nanoparticles has much higher photocatalytic activity that pure anatase or pure rutile[1-30]. For example, Degussa P25 consisting of a mixture of anatase and rutile mineral phases posses superior photocatalytic activity and has widely used as a gold standard for the comparison of reactivity[1-8].

Many researchers have proposed that the high photocatalytic activity of mixed-phase titania originates from the spatial separation of photogenerated charge carriers, but there is disagreement about the direction of charge transfer. Tada and co-workers have prepared a patterned anatase/rutile bilayer-type film and found that silver photodeposition occurred preferentially at the boundary toward the rutile layer[9]. So they have suggested that some of the photogenerated electrons are transferred from the conduction band of anatase to that of rutile based on the position of the conduction band edge of anatase relative to that of rutile. However, Gary and co-workers argued that the reactions such as the reduction of silver are dependent not only on the electron transfer but also adsorption events[4]. They have reported that in a mixed-phase material (P25), electrons trapping on the anatase surface was observed under visible light illumination by EPR measurements, indicating the electron transfer from rutile to anatase occurred[3]. They have proposed a model where rutile acts as an antenna to extend the photoactivity into visible wavelength and the structural arrangement of the similarly sized titania crystallites creates catalytic "hot spots" at the rutile-anatase interface. Matsumura and co-workers observed that oxidation and reduction reactions occurred on rutile and anatase particles, respectively, when mixed-phase titania was used in photocatalytic oxidation of naphthalene[10]. They have suggested that electrons are transferred from rutile particles to anatase particles *via* thermal activation. Smirniotis and co-workers have proposed that the conduction band energy increase in the space charge layer of anatase stops the electrons going from anatase to rutile, but the holes in anatase particles can be transferred to rutile particles through the valance band bending[6]. Serpone and co-workers have suggested that photogenerated electrons in the rutile domains, which can in essence be considered as surface defects in the P25 specimen, may spillover onto the anatase component[7].

Mixed-phase titania has been prepared by calcining amorphous-$TiO_2$[11-17] or anatase-$TiO_2$[10,18] or the mixture of amorphous-$TiO_2$ with rutile[19,20] or the mixture of anatase with rutile[21-24], physically mixing anatase with rutile[10,25], hydrothermal[25-28], gas-phase pyrolysis[29], low-temperature dissolution-reprecipitation[30], magnetron sputtering[15,31] and two-step method consisting of sputter deposition and subsequent sol-gel processing[9].

Different researchers reported different optimum rutile contents corresponding to the maximum photocatalytic activity, which are 11.2 wt %[29], 12 wt %[27], 15 wt %[28], 22.6 wt %[18],

24.5 wt %[12], 25.8 wt %[25], 28 wt %[14], 30 wt %[26], 40 wt %[23], 42.4 wt %[17], 43 wt %[16], 50 wt %[30], 78 wt %[15], 90 wt %[10] and 99.5 wt %[19], respectively.

From all above, it can been found that the mechanism of the synergetic effect between anatase and rutile is not fully understood. Herein, In view of the theory of semiconductor physics, we give the electric field distribution in the transition region of the *n-n* anatase-rutile heterojunction by solving the Poisson equation, discuss the direction of charge transfer and explain the synergetic effect.

**Energy-band diagram:** The energy-band diagram for isolated rutile and anatase is shown in Fig. 1(a) where rutile and anatase are not yet in contact[32-34]. Upon contact, because of the flatband potential (which corresponds to the position of the Fermi level) of anatase having a energy of 0.2 eV above than the Fermi level of rutile[35], at an *n-n* heterojunction located at the juncture between anatase and rutile (anatase and rutile are both of *n*-type semiconductors[35-40]), the electrons keep on flowing from anatase (smaller work function) to rutile (larger work function) until the Fermi levels become coincident, creating an accumulation of negative charges in the rutile region and a positive section in the anatase region in the vicinity of the junction. This sets up an internal electrostatic field directed from the anatase region to the rutile region, creating an energy barrier for the electron transfer from anatase to rutile. The band diagram for the *n-n* anatase-rutile heterojunction at equilibrium is shown in Fig. 1(b). In Fig. 1[32,33], the subscripts 1 and 2 refer to rutile and anatase; $\chi$ is electron affinity of the semiconductors; $\Phi$ is work function; $\varphi$ is electrostatic potential; $\varphi_D$ is diffusion potential (0.2 V for the *n-n* anatase-rutile heterojunction)[35]; $E_F$ is Fermi level; q is electronic charge (absolute value); x is the coordinate giving the distance from the interface with positive values applying to depth into anatase; $E_c$ and $E_v$ are conduction and valence band edge, respectively.

In the condition of equilibrium the electron energy level of rutile will be raised, because of the negative charge it has acquired. In the meantime, the electron energy level of anatase will be dropped, because the negative charge has spread and disappeared.

**Electric field distribution in the transition region:** Kumar[32] and Cservey[33] have already solved the Poisson equation for the transition region of an abrupt *n-n* heterojunction and arrived at the same conclusions. In this paper, we present the main deductive steps and conclusions in their articles and apply the conclusions to the anatase-rutile heterojunction.

In region 1 ($x_1x_o$), Poisson's equation takes the following form[32,33]:

$$\frac{d^2\varphi}{dx^2} = \frac{q}{\varepsilon_1\varepsilon_0}[N_{C1}\exp\{\frac{q\varphi(x) - q\varphi(x_1) + \chi_1 - \phi_1}{kT}\} - N_{D1}] \quad (1)$$

where k is Boltzmann constant, T is absolute temperature (assuming T = 298 K in this study), $\varepsilon_0$ is the permittivity of the vacuum, $\varepsilon$ is the dielectric constant ($\varepsilon_1 \approx 100$, $\varepsilon_2 \approx 30$)[36] and ND is the donor density.

At this point we introduce the notion[32],

$$\beta_1(x) = \frac{q}{kT}[\varphi(x) - \varphi(x_1)] \quad (2)$$

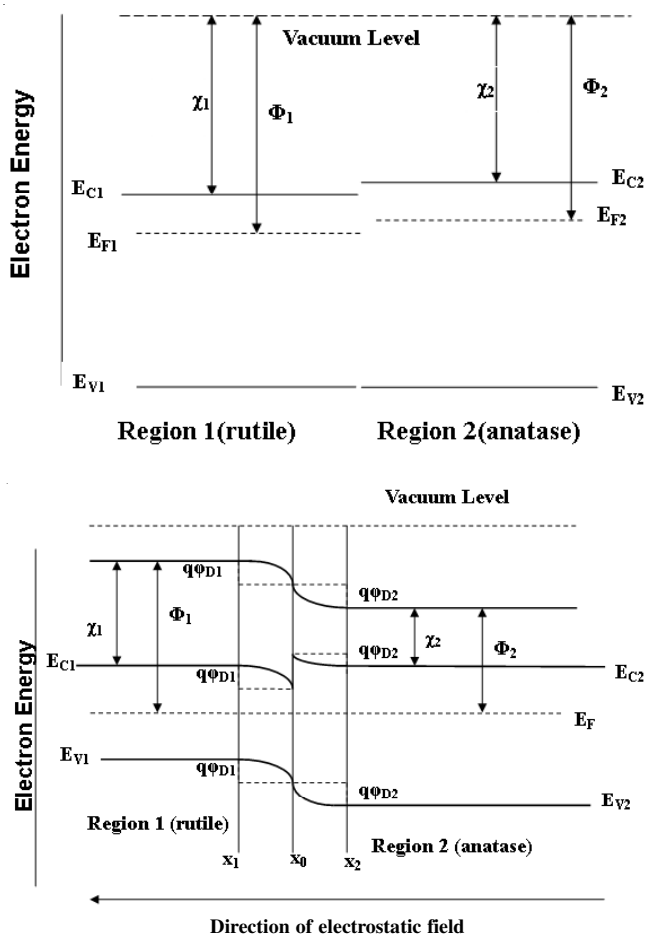


Fig. 1. Energy band diagrams of mixed-phase titania before (a) and after (b) the formation of *n-n* heterojunction

$$\beta_2(x) = \frac{q}{kT}[\varphi(x_2) - \varphi(x)] \quad (3)$$

$$L_{1,2}^2 = \frac{\varepsilon_0\varepsilon_{1,2}kT}{2q^2N_{D1,2}} \quad (4)$$

From eqn. 1, we have[32],

$$I(\beta_1,\beta_{1m}) = \int_{\beta_1}^{\beta_{1m}}[\exp(\beta_1) - \beta_1 - 1]^{-\frac{1}{2}}d\beta_1 = \frac{x_0 - x}{L_1} \quad (5)$$

The upper bound of $\beta_1$ in eqn. 5 is denoted by[32],

$$\beta_{1m} = \frac{q}{kT}[\varphi(x_0) - \varphi(x_1)] = \frac{q}{kT}\varphi_{D1} \quad (6)$$

where $\varphi_{D_1}$ is the portion of the diffusion potential supported by rutile. Similarly, we have[32],

$$\beta_{2m} = \frac{q}{kT}[\varphi(x_2) - \varphi(x_0)] = \frac{q}{kT}\varphi_{D2} \quad (7)$$

$$\beta_{1m} + \beta_{2m} = \beta_m = \frac{q}{kT}\varphi_D \quad (8)$$

$$\frac{\exp(\beta_{1m}) - \beta_{1m} - 1}{\exp(-\beta_{2m}) + \beta_{2m} - 1} = \frac{\varepsilon_2 N_{D2}}{\varepsilon_1 N_{D1}} \quad (9)$$

Assuming $N_{D_1}$ equals to $7 \times 10^{23}$ $m^{-3}$, $N_{D_2}$ equals to $10^{25}$ $m^{-3}$ (case 1)[36]. Then from eqn. 9, we have $\varphi_{D_1} = 0.077$ V. Then

from eqn. 6, we have $\beta_{1m} = 3.0$. Then from eqns. 5 and 4, we can obtain the variation of $\beta_1$ with the distance from the interface shown in Fig. 2.

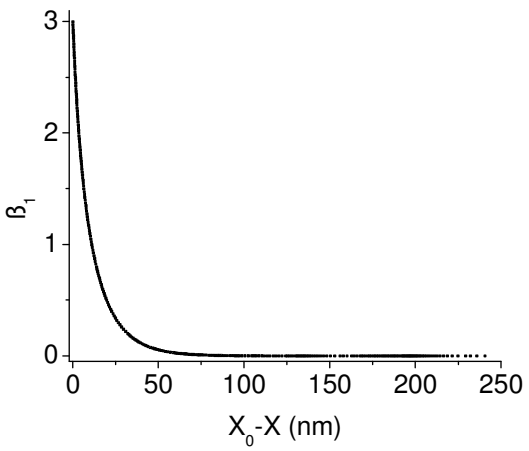


Fig. 2. Variation of potential inside rutile with the distance from the interface

For the electric field (E)

$$E = -\frac{d\varphi}{dx} = -\frac{kT}{q}\frac{d\beta_1}{dx} = -\frac{kT}{q}\frac{\Delta\beta_1}{\Delta x} = -\frac{kT}{q}\frac{\beta_{1,(i+1)} - \beta_{1,i}}{x_{1,(i+1)} - x_{1,i}} \quad (10)$$

($x_{1,(1+i)}$ and $x_{1,i}$ are the ordinates of two adjacent points of the curve in Fig. 2, respectively. $\beta_{1,(1+i)}$ and $\beta_{1,i}$ are the abscissas of two adjacent points, respectively).

Then from eqn. 10, we calculated the variation of E with the distance from the interface shown in Fig. 3. For simplicity, we omit the minus signs of E that represent the direction of electric field.

As indicated in Fig. 3, strong electric field exists in the transition region of the *n-n* anatase-rutile heterojunction, the field strengths at the interface are greater than $10^7$ V/m. Such a transition region can exert a very efficient force for photo-generated electron hole pair separation, resulting in greater photocatalytic activity.

Fig. 3(a) shows the electric field distribution in different cases. In case 2, $N_{D_1} = N_{D_2} = 10^{24}$ m$^{-3}$. In case 3, $N_{D_1}$ ($3.9 \times 10^{25}$ m$^{-3}$)[37] >> $N_{D_2}$ ($4.1 \times 10^{22}$ m$^{-3}$)[38]. In case 4, $N_{D_1}$ ($1.5 \times 10^{23}$ m$^{-3}$)[39] << $N_{D_2}$ ($8.36 \times 10^{25}$)[40]. As indicated from Fig. 3(a), if the donor density in one region is much less than that in another region ($N_{D_1} << N_{D_2}$ (case 4) or $N_{D_2} << N_{D_1}$ (case 3)), the electric field distribution in this region is much broader than that in another region.

If the value of $N_{D_1}$ keeps constant, when $N_{D_2}$ increases (case 5) or decreases (case 6), the electric field distribution in region 2 will narrow or broaden, respectively, while the electric field distribution in region 1 changes slightly. Similarly, if the value of $N_{D_2}$ keeps constant, when $N_{D_1}$ increases (case 7) or decreases (case 8), the electric field distribution in region 1 will narrow or broaden, respectively, while the electric field distribution in region 2 changes slightly. The results are shown in Fig. 3(b). In case 5 and 6, $N_{D_2}$ is $8.36 \times 10^{25}$ m$^{-3}$ [40] and $4.1 \times 10^{22}$ m$^{-3}$ [38], respectively. In case 7 and 8, $N_{D_1}$ is $3.9 \times 10^{25}$ m$^{-3}$ [37] and $1.5 \times 10^{23}$ m$^{-3}$ [39], respectively. The parameters and results of the *n-n* anatase-rutile heterojunction in the different cases are summarized in Table-1.

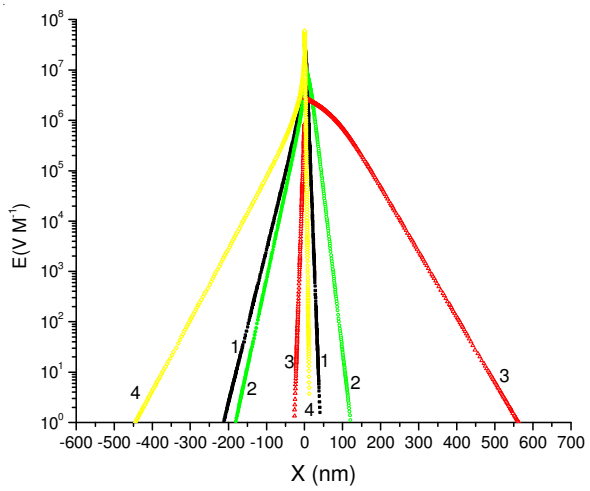


(a)

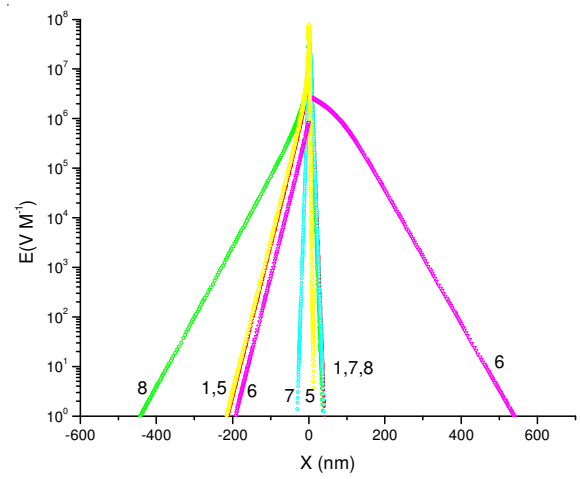


(b)

Fig. 3. Electric field of the n-n anatase-rutile heterojunctions with the different donor densities. The numbers 1-8 represent the different cases. (a) In case 1, $N_{D1} = 7 \times 10^{23}$ m$^{-3}$, $N_{D2} = 10^{25}$ m$^{-3}$; in case 2, $N_{D1} = N_{D2} = 10^{24}$ m$^{-3}$; in case 3, $N_{D1} = 3.9 \times 10^{25}$ m$^{-3}$, $N_{D2} = 4.1 \times 10^{22}$ m$^{-3}$; in case 4, $N_{D1} = 1.5 \times 10^{23}$ m$^{-3}$, $N_{D2} = 8.36 \times 10^{25}$ m$^{-3}$. (b) In case 5, $N_{D1} = 7 \times 10^{23}$ m$^{-3}$, $N_{D2} = 8.36 \times 10^{25}$ m$^{-3}$; in case 6, $N_{D1} = 7 \times 10^{23}$ m$^{-3}$, $N_{D2} = 4.1 \times 10^{22}$ m$^{-3}$; in case 7, $N_{D1} = 3.9 \times 10^{25}$ m$^{-3}$, $N_{D2} = 10^{25}$ m$^{-3}$; in case 8, $N_{D1} = 1.5 \times 10^{23}$ m$^{-3}$, $N_{D2} = 10^{25}$ m$^{-3}$

TABLE-1
PARAMETERS AND RESULTS OF THE *n-n* ANATASE-RUTILE HETEROJUNCTION IN THE DIFFERENT CASES

| Case | $N_{D_1}$ (m$^{-3}$) | $N_{D_2}$ (m$^{-3}$) | $\varphi_{D_1}$(V) | $\varphi_{D_2}$(V) | $\beta_{1m}$ | $\beta_{2m}$ |
|---|---|---|---|---|---|---|
| 1 | $7\times10^{23}$ | $10^{25}$ | 0.077 | 0.123 | 3.00 | 4.79 |
| 2 | $10^{24}$ | $10^{24}$ | 0.036 | 0.164 | 2.84 | 4.16 |
| 3 | $3.9\times10^{25}$ | $4.1\times10^{22}$ | 0.002 | 0.198 | 0.06 | 7.72 |
| 4 | $1.5\times10^{23}$ | $8.36\times10^{25}$ | 0.141 | 0.059 | 5.49 | 2.30 |
| 5 | $7\times10^{23}$ m$^{-3}$ | $8.36\times10^{25}$ | 0.115 | 0.085 | 4.48 | 3.31 |
| 6 | $7\times10^{23}$ m$^{-3}$ | $4.1\times10^{22}$ | 0.011 | 0.189 | 0.44 | 7.34 |
| 7 | $3.9\times10^{25}$ | $10^{25}$ | 0.021 | 0.179 | 0.82 | 6.97 |
| 8 | $1.5\times10^{23}$ | $10^{25}$ | 0.105 | 0.095 | 4.09 | 3.70 |

Although many researchers have found the synergistic effect between anatase and rutile, different researchers reported different optimum rutile content corresponding to the maximum photocatalytic activity, which is noted to be within the range of 11.2-99.5 wt %[10,12,14-19,23,25-30]. This range is large and may be attributed to the different donor densities of mixed-

phase titania since the electric field distribution depends on the donor densities. Certainly, other parameters such as crystallite size, surface area, density of surface hydroxyl groups, secondary particle size *etc*., are also related to the photocatalytic activity[14-31].

As to the direction of the charge transfer, some researchers have suggested that the photogenerated electrons migrates from rutile to lower energy anatase trapping sites[3-5,7,10] or the photogenerated holes in the anatase phase transfer to rutile[6] while others have suggested that the photogenerated electrons in the anatase phase transfer to rutile based on the position of the conduction band edge of anatase relative to that of rutile[9,31]. In view of the theory of semiconductor physics[32,33,41], we suggest that the electrons flow from anatase to rutile when rutile is in close contact with the anatase. Once a stable *n-n* heterojunction has formed between rutile and anatase, under illumination, the photogenerated electrons will migrate from rutile to anatase while the photogenerated holes will migrate from anatase to rutile under the influence of the internal electrostatic field in the *n-n* heterojunction region. We suggest here, that the internal electrostatic force separates the photogenerated electrons and holes spatially and this is considered as the main effect, rather than the previously published concepts, like antenna effect[3], thermal activation[10], the valance band bending[6] or spillover effect[7]. Because the conduction band of anatase has been considered to locate at a higher energy position than that of rutile by about 0.2 eV, Matsumura *et al*.[10] thought that this relationship of the energy levels is disadvantageous to the electron transfer from rutile particles to anatase particles. Gray *et al*.[15] advanced that since the trapping site is 0.8 eV lower in energy than the anatase conduction band and is also below (*ca.* 0.6 eV) the rutile conduction band, the electron transfer from rutile to anatase is energetically allowed. In fact, the positions of the conduction band that they discussed are that of isolated rutile and anatase (Fig. 1(a)). The Fermi levels of mixed-phase titania are coincident (*i.e.*, the Fermi level is constant throughout the material) after the formation of the *n-n* anatase-rutile heterojunction (Fig. 1(b)).

## Conclusion

In view of the theory of semiconductor physics, we give the electric field distribution in the transition region of the *n-n* anatase-rutile heterojunction by solving the Poisson equation. Strong electric field exists in the transition region and can exert a very efficient force for photogenerated electron hole pair separation, resulting in greater photocatalytic activity. The electric field distribution depends on the donor densities. The electrons flow from anatase to rutile when rutile is in close contact with the anatase. Once a stable *n-n* heterojunction has formed between rutile and anatase, under illumination, the photogenerated electrons will migrate from rutile to anatase while the photogenerated holes will migrate from anatase to rutile. Of course, the involved mechanism would become more complicated when the surface state and defects were taken into account. Further detailed information about the anatase-rutile heterojunction and further investigations are needed, in order to solve questions about the photocatalytic process.

## REFERENCES


1. R.I. Bickley, T. Gonzalez-Carreno, J.S. Lees, L. Palmisano and R.J.D. Tilley, *J. Solid State Chem.*, **92**, 178 (1991).
2. G. Li, N.M. Dimitrijevic, L. Chen, J.M. Nichols, T. Rajh and K.A. Gray, *J. Am. Chem. Soc.*, **130**, 5402 (2008).
3. C.D. Hurum, K.A. Gray, T. Rajh and M.C. Thurnauer, *J. Phys. Chem. B*, **109**, 977 (2005).
4. C.D. Hurum, A.G. Agrios, S.E. Crist, K.A. Gray, T. Rajh and M.C. Thurnauer, *J. Electron Spectrosc. Rel. Phenom.*, **150**, 155 (2006).
5. C.D. Hurum, A.G. Agrios, K.A. Gray, T. Rajh and M.C. Thurnauer, *J. Phys. Chem. B*, **107**, 4545 (2003).
6. B. Sun, A.V. Vorontsov and P.G. Smirniotis, *Langmuir*, **19**, 3151 (2003).
7. A.V. Emeline, L.G. Smirnova, G.N. Kuzmin, L.L. Basov and N. Serpone, *J. Photochem. Photobiol. A Chem.*, **148**, 97 (2002).
8. T. Ohno, K. Sarukawa, K. Tokieda and M. Matsumura, *J. Catal.*, **203**, 82 (2001).
9. T. Kawahara, Y. Konishi, H. Tada, N. Tohge, J. Nishii and S. Ito, *Angew. Chem. Int. Ed.*, **41**, 2811 (2002).
10. T. Ohno, K. Tokieda, S. Higashida and M. Matsumura, *Appl. Catal. A*, **244**, 383 (2003).
11. J. Yu, J.C. Yu, W. Ho and Z. Jiang, *New J. Chem*., **26**, 607 (2002).
12. W. Wang, M. Gu and Y. Jin, *Mater. Lett.*, **57**, 3276 (2003).
13. Y. Sung, J. Lee and W. Chae, *Cryst. Growth Des.*, **6**, 805 (2006).
14. L. Chen, J. Zhu, Y. Liu, Y. Cao, H. Li, H. He, W. Dai and K. Fan, *J. Mol. Catal. A*, **255**, 260 (2006).
15. G. Li, L. Chen, M. Graham and K.A. Gray, *J. Mol. Catal. A*, **275**, 30 (2007).
16. K. Lv, J. Yu, K. Deng, X. Li and M. Li, *J. Phys. Chem. Solids*, **71**, 519 (2010).
17. C.K. Chan, J.F. Porter, Y.G. Li, W. Guo and C.M. Chan, *J. Am. Ceram. Soc.*, **82**, 566 (1999).
18. S. Bakardjieva, J. Šubrt, V. Štengl, M.J. Dianez and M.J. Sayagues, *Appl. Catal. B*, **58**, 193 (2005).
19. T. Kawahara, T. Ozawa, M. Iwasaki, H. Tada and S. Ito, *J. Colloid Interf. Sci.*, **267**, 377 (2003).
20. J. Zhang, Q. Xu, Z. Feng, M. Li and C. Li, *Angew. Chem. Int. Ed.*, **47**, 1766 (2008).
21. Z.Y. Liu, X.T. Zhang, S. Nishimoto, M. Jin, D.A. Tryk, T. Murakami and A. Fujishima, *Langmuir*, **23**, 10916 (2007).
22. G. Li, S. Ciston, Z.V. Saponjic, L. Chen, N.M. Dimitrijevic, T. Rajh and K.A. Gray, *J. Catal.*, **253**, 105 (2008).
23. A. Zachariah, K.V. Baiju, S. Shukla, K.S. Deepa, J. James and K.G.K. Warrier, *J. Phys. Chem. C*, **112**, 11345 (2008).
24. K.V. Baiju, A. Zachariah, S. Shukla, S. Biju, M.L.P. Reddy and K.G.K. Warrier, *Catal. Lett.*, **130**, 130 (2009).
25. M. Yan, F. Chen, J. Zhang and M. Anpo, *J. Phys. Chem. B*, **109**, 8673 (2005).
26. R.R. Bacsa and J. Kiwi, *Appl. Catal. B*, **16**, 19 (1998).
27. C. Wu, Y. Yue, X. Deng, W. Hua and Z. Gao, *Catal. Today*, **93-95**, 863 (2004).
28. V. Kolen'ko Yu, B.R. Churagulov, M. Kunst, L. Mazerolles and C. Colbeau-Justin, *Appl. Catal. B*, **54**, 51 (2004).
29. K.Y. Jung, S.B. Park and H.D. Jang, *Catal. Commun.*, **5**, 491 (2004).
30. P. Zhang, S. Yin and T. Sato, *Mater. Res. Bull.*, **45**, 275 (2010).
31. T. Miyagi, M. Kamei, T. Mitsuhashi, T. Ishigaki and A. Yamazaki, *Chem. Phys. Lett.*, **390**, 399 (2004).
32. R.C. Kumar, *Solid State Electron*, **11**, 543 (1968).
33. S.I. Cserveny, *Int. J. Electron*, **25**, 65 (1968).
34. S. Liu, J. Wu, X. Liu and R. Jiang, *J. Mol. Catal. A*, **332**, 84 (2010).
35. L. Kavan, M. Grätzel, S.E. Gilbert, C. Klemenz and H.J. Scheel, *J. Am. Chem. Soc.*, **118**, 6716 (1996).
36. M. Dolata, P. Kedzierzawski and J. Augustynski, *Electrochim. Acta*, **41**, 1287 (1996).
37. S.U.M. Khan and J. Akikusa, *J. Electrochem. Soc.*, **145**, 89 (1998).
38. R. Van de Krol, A. Goossens and J. Schoonman, *J. Electrochem. Soc.*, **144**, 1723 (1997).
39. P. Salvador, M.L. García González and F. Muñoz, *J. Phys. Chem.*, **96**, 10349 (1992).
40. F.Y. Oliva, L.B. Avalle, E. Santos and O.R. Cámara, *J. Photochem. Photobiol. A*, **146**, 175 (2002).
41. S. Liu, X. Liu, S. Chen and R. Jiang, *J. Alloys Compd.*, **506**, 877 (2010).